Nigerian Journal of Theoretical and Environmental Physics (NJTEP)
ISSN Online: 1597-9849
ISSN Print: 3026-9601
DOI: https://doi.org/10.62292/njtep.v3i1.2025.71
Volume 3(1), March 2025

A DFT Approach on the Impact of Hydrostatic Pressure on the Structural, Mechanical, Lattice dynamics, and Optical Characteristics of the Cubic Perovskite $RbTaO_3$

***[1]Aigbekaen Eddy Enorense and [2]Ighakpata Fidelia Chukwudumebi**

[1]Department of Physics, Igbinedion University, Okada, Benin City, Nigeria.
[2]Department of Physics, College of Education, Warri, Delta State.

[*]Corresponding author's email: aigbekaen.eddy@iuokada.edu.ng

ABSTRACT

The structural, mechanical, electrical, lattice dynamic, and optical features of the cubic perovskite RbTaO3 beneath pressure (0–150GPa) are scrutinized using ab-initio calculations established on the spin-polarized density functional theory (SP-DFT). In accordance with the lattice parameter-energy variation curve, the compound is none ferromagnetic nor non-magnetic. Mechanical stability criteria for cubic structures disclose that the material is both brittle and stable. In agreement with the Zener anisotropy factor data, the compound displays anisotropic performance between 0 and 40 GPa and isotropic performance above 40 GPa. It was also prominent to have a semiconductor character, as seen by the electrical band structures, and the band gap changed from an indirect one at 0 GPa to a direct one at 150 GPa as a consequence of pressure application. In view of this energy gap transition, $RbTaO_3$ is a likely material for use in photovoltaic, optoelectronic, and photochemical devices. The appearance of negative frequencies in the material makes it dynamically unstable, as can be seen from the phonon dispersion curves. The fundamental optical functions were considered, including the extinction coefficient (ω), optical conductivity, $\sigma(\omega)$, reflectivity $R(\omega)$, electron energy-loss spectrum $L(\omega)$, absorption coefficient spectrum $\alpha(\omega)$, and refractive index $n(\omega)$. The optical characteristic indicates that the visible-ultraviolet spectrum is where cubic RbTaO3 is active.

Keywords:
Half-Heusler,
Band gap,
Bulk modulus,
Semiconductor,
Dielectric function,
Refractive index.

INTRODUCTION

One of the most predominant structural types in solid-state inorganic chemistry is the perovskite. A three-dimensional fabric of corner-sharing BX_6 octahedral with ABX_3 stoichiometry form the model perovskite structure. The BX_3 network creates 12 coordinate holes, which are filled by the A-site cation, which is surrounded by 12 anions distributed equally apart. The bulk of the metallic ions found in the periodic table, along with several rare anions, can be found in the perovskite structure. Although the perovskite structure is also known for heavier halides, the higher number of perovskite compounds are oxides or fluorides (Lufaso and Woodward, 2001). The much common structure amidst ternary oxides is the perovskite, which has been wholly studied using first-principles calculations. Due to the oxides' special properties, a large number of works in this area have been reviewed. However, amidst perovskites, cubic perovskite solids are extremely stable and have the model structure, crystallizing with a space group of Pm-3m (# 221). Perovskites and their derivatives have complex and conceivable vital properties.

In current decades, a number of topics have drawn the interest of scholars worldwide, including ferromagnetism (Khandy and Gupta, 2017), superconductivity (Schneemeyer *et al.*, 1987; Iyorzor *et al.*, 2018; Okunzuwa and Aigbekaen, 2021; Aigbekaen and Ighrakpata, 2022), spin-polarization (Rhazouani *et al.*, 2016), immense magnetoresistance (Raveau *et al*., 1998), and thermoelectricity (Reshak, 2016). Moreover, Bouadjemi *et al*. (2015), insinuated that the $NdMnO_3$ perovskite would be a likely material for spintronic and optoelectronic devices after theoretically collating a variety of characteristics, including optical, magnetic, and structural characteristics. Evaluation has also been done on $BaTiO_3$ as a propable material for ceremic capacitors and electro-optic devices (Pithan *et al.*, 2005; Tian *et al*., 2009; Tsurumi *et al*., 2002). The most likely material for electrically tunable devices is ferroelectric

ceramics, which have been employed in microwave devices such phase shifters, varactors, tunable oscillators, and detectors (Jindal *et al*., 2018). Research have been carried on the thermoelectric and magnetic characteristics of tantalum-based perovskite oxides $XTaO_3$ (X = Rb, Fr) in cubic phase (Hussain *et al*., 2021). Both the direct band gap of 1.08 eV in $FrTaO_3$ and the indirect energy band gap of 1.12 eV in $RbTaO_3$ were important band gap values. The FP-LAPW method was applied in the study of Sarwan et al.,2020 to examine the electrical, elastic, and structural attribute of $RbTaO_3$. In a perovskite structure, the structural character shows that it is stable. The indirect band gap of $RbTaO_3$ is disclosed by its electrical characteristics. The expected elastic properties of the present chemical confirmed its brittle nature. Using the density functional theory (DFT), the $NdInO_3$ cubic structure was completely examined (Butt *et al*., 2020). This material may be ideal for ultraviolet-optical devices in view of its wide absorption range in the UV region, according to the research. $Ba_{1-x}Ca_x$ TiO_3 and $Ba_{1-x}Sr$ $_xTiO_3$ (x=0.4,0.6) were studied for their structural, electrical, and optical characteristics using DFT-GGA calculations in the ABINIT code (Tahiri et al., 2018). According to the outcome, an indirect transition was observed at M-point. The $Ba_xSr_{1-x}TiO_3$ compound's microstructure, dielectric, and mechanical losses were seen (Cheng *et al*., 2002). For phase transitions in $Ba_xSr_{1-x}TiO_3$, the dielectric constant/elastic modulus loss peak rate was affected by the size and formation of the grains. The influence of pressure (0-150 GPa) on $RbTaO_3$ perovskite is examined using DFT, and a transition from indirect to direct band gap is realize (Hassan *et al*., 2021). Electrical, optical, and thermoelectric properties were inspected in relation to band gap variation.

Its lattice dynamic and structural stabilities, including the pressure at which it will become unstable, were not discussed in this latest report or any earlier research on $RbTaO_3$ perovskite, we use the Quantum ESPRESSO package to inquire how hydrostatic pressure affects the structural, electrical, mechanical, lattice dynamics, and optical characteristics of the cubic perovskite $RbTaO_3$.

MATERIALS AND METHODS

Computational details

The various attributes were examined using the First Principles method based on (SP-DFT) (Giannozzi *et al*., 2009) in the QUANTUM ESPRESSO (QE) algorithm. The calculation was accomplished using the Projected Augumented Wave Pseudo Potential (PAWPP) (Perdew *et al*., 1996). Bonding, magnetic properties, and the exchange interaction between electrons were all handled using the Perdew-Burke-Ernzerhof (GGA) approach (Perdew *et al*., 1997). . Before determining on the proper values for the computations, convergence tests were performed for the kinetic energy cut-off and the k-points mesh samplings. Convergence thresholds of 10^{-8} eV/atom for the total energy and a kinetic energy cut-off of 90Ry were employed in the Monkhorst-Pack format with a 9x9x9 framework. Rb_5S_1, $Ta_5d_36S_2$, and $O_2S_22p_4$ are the pseudo-atomic configurations that were utilised as valence electrons, respectively. Figure 1 illustrates the cubic crystal structure of $RbTaO_3$. In the Pm-3m (221) space group, the atoms Rb, Ta, and O are located in Wyckoff positions 1a(0,0,0), 1b(1/2,1/2,1/2), and 3c(1/2,1/2,0), respectively.

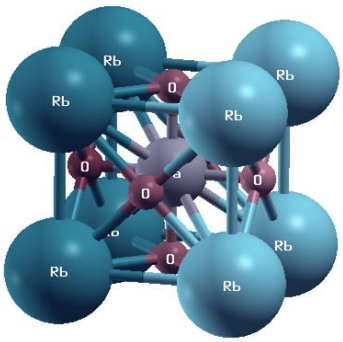

Figure 1: Structure of RbTaO3

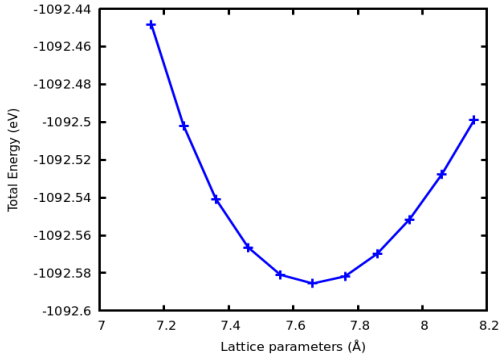

Figure 2: Lattice parameters Vs Energy of RbTaO3

RESULTS AND DISCUSSION

Structural and Mechanical Properties

The structural and mechanical feature of the RbTaO3 perovskite's ground state configuration were scrutinized. The total energy minimization of the compound in response to the alteration of the lattice parameters allowed for the geometric optimization of the cubic perovskite structure in both ferromagnetic (FM) and non-magnetic (NM) states. The equilibrium lattice constant a, bulk modulus B, and its pressure derivative B' were determined during the self-consistent calculation and are shown in Table. Furthermore, Figure 2 (Energy Vs Lattice parameter curve) for the compound showed that it is neither ferromagnetic nor non-magnetic. Confirming the geometric stability of perovskite structures requires calculating the tolerance

factor, or "t." In fact, it is an empirical metric that establishes a link between the stability of a perovskite and its chemical composition (Ilyas *et al*., 2021). The Goldschmidt tolerance factor "t" of an ABO_3 perovskite structure can be computed using the following formula, where r_A, r_B and r_O are the ionic radii of atoms A, B (cations), and O (anion).

$$t = \frac{(r_A + r_O)}{\sqrt{2}(r_B + r_O)} \quad (1)$$

The range of tolerance is $0.8 < t < 1.04$. $\mu = r_B/r_0$ is the definition of the octahedral factor, another metric for forecasting structural stability. When the octahedral factor range for perovskites is between 0.414 and $\mu < 0.732$, the structure is stable. Remarkably, $RbTaO_3$ has an octahedral factor μ of 0.5151 and a tolerance factor t of 0.9864. These are symptoms of the compound's stability. Elastic constants and particular structural characteristics have an inevitable role in determining the mechanical stability of materials in solids (Wu *et al*., 2007). The subsequent criteria are used to test the stability of cubic phases: $C_{11} + 2C_{12} > 0$, $C_{11} - C_{12} > 0$, $C_{44} > 0$, and $C_{11} > 0$ (Sinko and Smirnow, 2002). The materials are elastically stable opposed to deformation, based on observation. The following elements should be taken into consideration in order to confirm the brittleness and ductility of materials: the Cauchy pressure ($C_{12} - C_{44}$), Pugh's index (B/G), and Poisson's ratio (υ) (Iyorzor *et al*., 2018; Bakare *et al*., 2017). When determining the mechanical properties of solids, the bulk B, Young E, and Shear G moduli are essential variables. The B/G ratio's threshold value for distinguishing between a material's brittleness and ductility is roughly 1.75 (Pugh, 1954). Table 3 this signifies that the compound is fragile because the B/G ratio values are less than 1.75. The type of bonding forces in materials is disclosed by the Poisson's ratio, which ranges from 0 to 0.5 (Boucetta, 2014). The compound's degree of flexibility is important. The Cauchy relation is another vital structural metric that characterizes the brittleness and ductility of materials. A positive value denotes that the material is ductile; a negative value indicates that it is brittle. Based on the information supplied, the chemical is obviously fragile. Since the values are getting closer to unity, the Zener anisotropy, A, results denotes that the compound is anisotropic within the pressure range of 0GPa to 40GPa. High elastic anisotropy is illustrated by this, whereas isotropic property is displayed above 40GPa.

Table 1: The Structurer properties: the a (Å), B (GPa), and band gap near Fermi energy Eg (eV) within pressure range of (0-150GPa)

	0GPa	20GPa	40GPa	100GPa	150GPa
a (Å)	4.0677	3.9353	3.8517	3.6852	3.5922
B (GPa)	182.56	259.78	327.02	507.51	641.28
Eg (eV)	2.0556	2.2679	2.3931	2.6035	2.6714

Electronic Properties

Under the influence of hydrostatic pressure (0–150 GPa), the electronic band structures of the cubic perovskite $RbTaO_3$ are determined to be completely semiconductors, with the Fermi energy level situated at the largest valence band. Given the extreme pressures, the 0GPa has an indirect band gap of 2.0555eV, with the greatest occupied valence band at M-point and the lowest unoccupied one in the conduction band at Γ-point. The lowest unoccupied conduction band and the highest occupied valence band are both situated at the Γ-point for 150GPa, suggesting a direct band gap of 2.6714eV. As the pressure rises beyond 150GPa a transition from indirect to a direct band gap started manifesting, and this transformation became very obvious at 150GPa as presented in Figure 4(a and b).

In the work of Hassan *et al*. (2021), the band structure for $RbTaO_3$ was computed using mBJ potential as implemented in Wien2K, at P = 0GPa an indirect band gap was obtained and at P = 75GPa a direct band gap was obtained. The transformation occurred at 75GPa, rather than the 150GPa reported in this paper, due to the use of PBE-GGA functional as implemented in the Quantum ESPRESSO code. The existence of this transformation in the energy gap makes $RbTaO_3$ a promising candidate for optoelectronic, photovoltaic and photochemistry devices applications.

Semiconductors must have an ideal band gap of greater than 1.4 and less than 3.0 eV in order to be used in photovoltaic and photochemical applications (Azzouz *et al*., 2019). Additionally, the partial densities of states (PDOS) for the compound's different pressures have been computed and are displayed in Figure 5(a-b). The PDOS plot's objective is to provide insight into the kind of bonding that exists between the orbitals and how each orbital affects the DOS.

The Ta-5d orbital made the most contribution to the conduction band at 0GPa, whereas the O-2p orbital made the smallest. Their influence began at roughly 1.9 eV, which is far from the Fermi energy threshold. Similar to this, each of the three orbitals contributed differently in the valence band, with the O-2p orbital contributing the most and the Rb-3p orbital contributing the least. The presence of a strong covalent bond was found. The orbital contribution declined nearly entirely in the conduction band, with the exception of the Ta-5d

orbital. The high pressure caused an increase in the repulsive force between atoms. This led to an increase in the band gap between the valence and conduction bands.

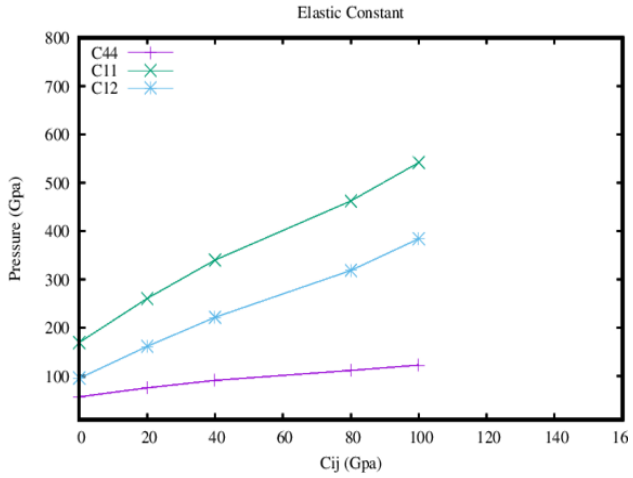

Figure 3: Pressure vs Elastic constants

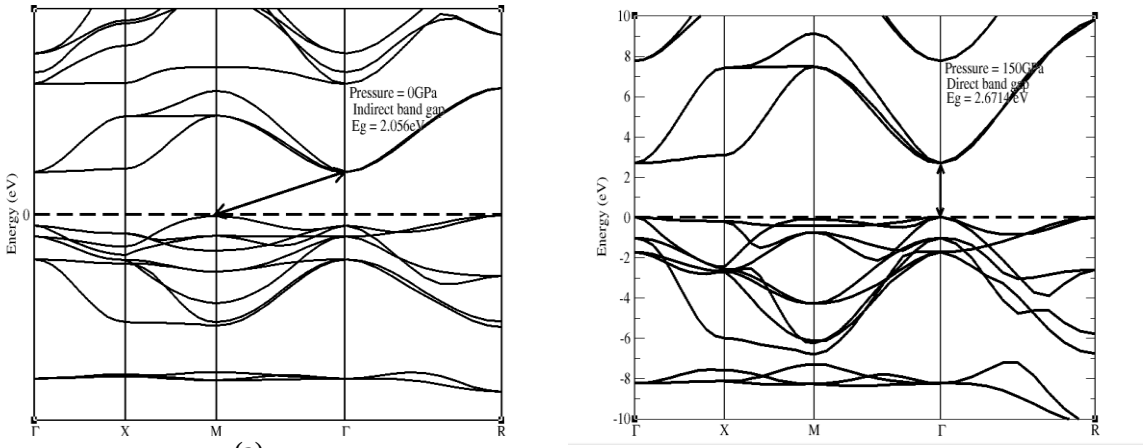

(a) (b)

Figure 4 (a-b): Electronic band structures of RbTaO3 for pressures (a) 0GPa and (b) 100GPa

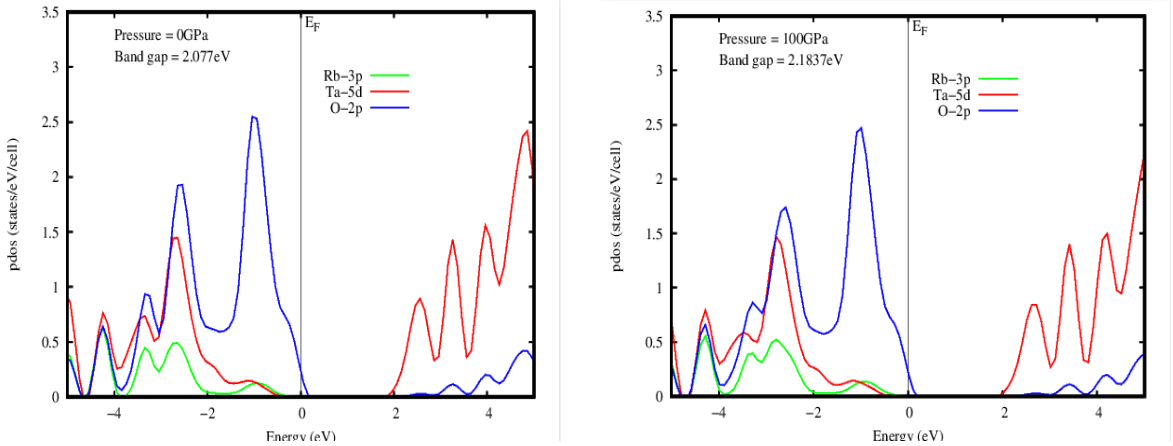

(a) (b)

Figure 5: The PDOS of RbTaO3 for pressures (a) 0GPa and (b) 100GPa

Vibrational properties

The phonon spectra of the different pressures (0-100GPa) were calculated in order to investigate the vibrational characteristics of the $RbTaO_3$ molecule. We employed the Thermo_pw package, a code that computes the physical properties of materials using Quantum ESPRESSO routines as the underlying engine. The phonon dispersion curves along the $\Gamma - X - M - \Gamma - R - X$ high symmetry directions are displayed in Figure 6(a–b). The finding of imaginary (negative) frequencies in the compound's Brillouin zone, which suggest that it is dynamically unstable, was one noteworthy feature.

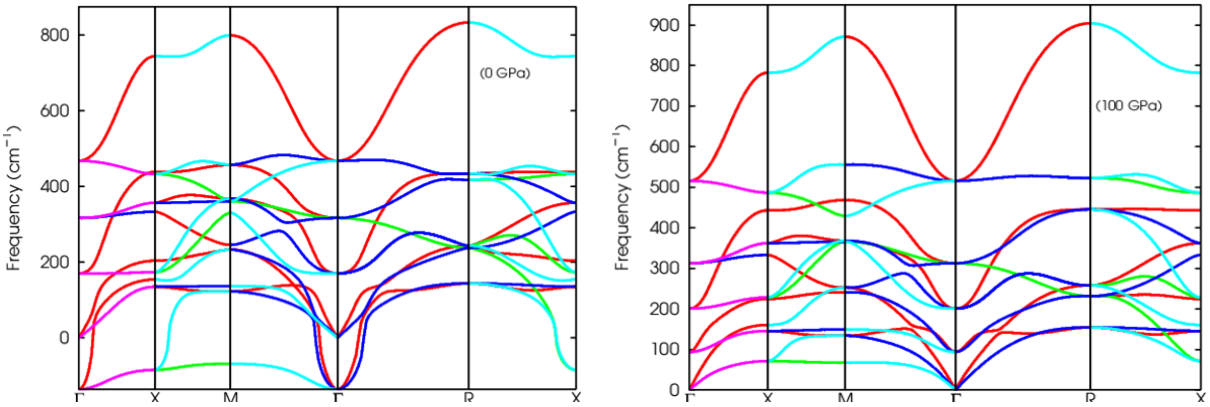

Figures 6 (a-b): Phonon dispersion curves along symmetry of $RbTaO_3$ at pressure (0GPa and 100GPa)

Optical properties

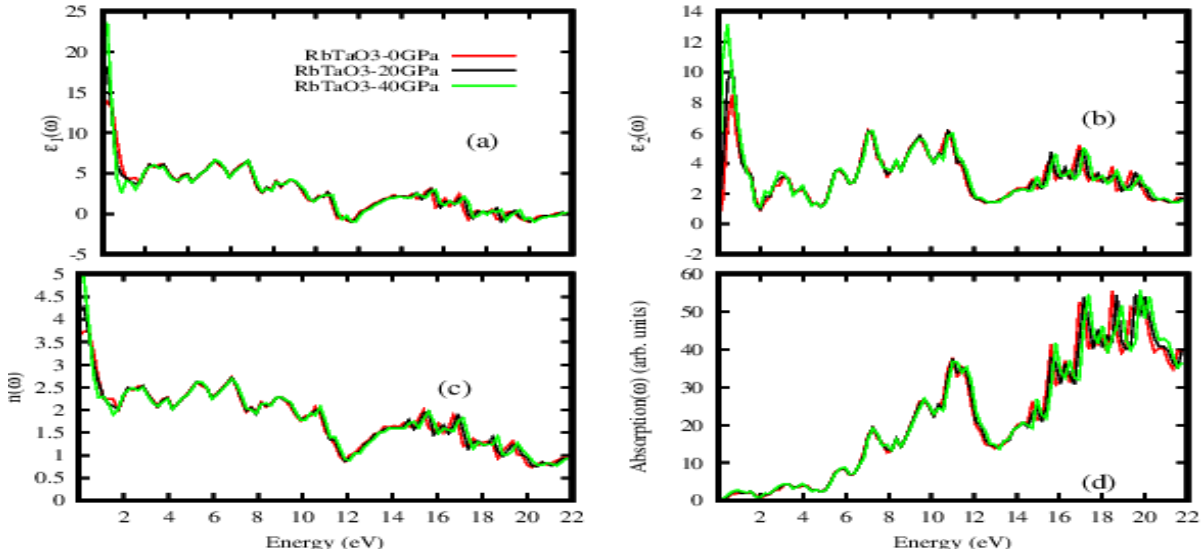

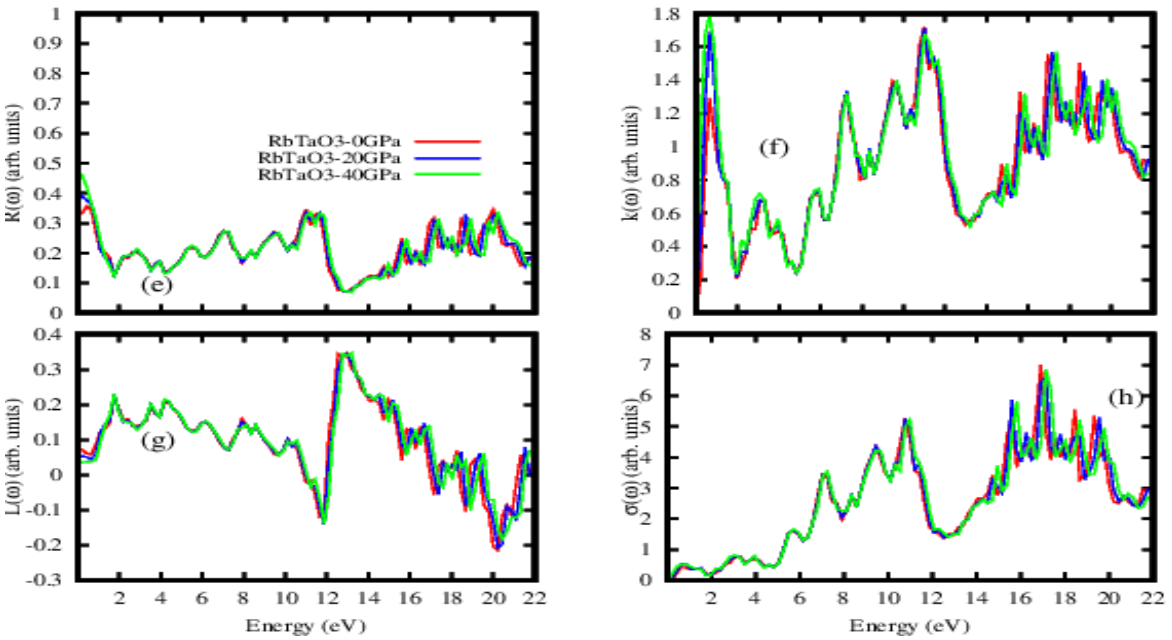

Figure 7(a-g): (a) Real part of the dielectric function $\varepsilon_1(\omega)$, (b) Imaginary part of the complex dielectric function $\varepsilon_2(\omega)$, (c) refractive index (n(ω), (d) absorption coefficient spectrum α(ω), (e) reflectivity ($R(\omega)$, (f) extinction coefficient ($k(\omega)$, (g) electron energy-loss spectrum ($L(\omega)$, (h) optical conductivity σ(ω).

Figure 7(a-g) shows the optical characteristics of the $RbTaO_3$ compound under hydrostatic pressure in the range of 0–18.4eV. The complex dielectric function $\varepsilon(\omega) = \varepsilon_1(\omega) + i\varepsilon_2(\omega)$ is used to compute the optical properties, where $\varepsilon(\omega)$ denotes the interaction of incoming radiation with matter. A system's linear reaction to external electromagnetic radiation is described by the complex dielectric function. The dispersion of the imaginary part of the complex dielectric function $\varepsilon_2(\omega)$ is computed using the momentum matrix elements between the occupied and unoccupied wave functions, and the Kramers–Kronig transformation is employed to compute the real part of the dielectric function $\varepsilon_1(\omega)$ (Hu *et al*., 2007) . In the zero frequency limits, the electronic component of the static dielectric constant, or the real part of the dielectric constant, is a significant value. For 0 GPa, 20 GPa, and 40 GPa, the static dielectric constants are 13.48, 17.27 and 23.96, respectively. Additionally, the full $\varepsilon_1(\omega)$ spectrum is suppressed when the pressure is raised above 0GPa; it decays with pressure. When compared to the literature, these findings are very similar (Sarwan *et al*., 2020). The imaginary part of the compound's dielectric function $\varepsilon_2(\omega)$ spectra shows a maximum peak at 0 GPa at 8.37 eV, 20 GPa at 9.88 eV and 40 GPa at 12.97 eV, respectively. The peak then diminishes linearly as the pressure increases. The imaginary dielectric constant $\varepsilon_2(\omega)$ shows larger energy shifts as external pressure increases. The real and imaginary parts of the dielectric function can be used to calculate the fundamental optical functions, including the refractive index n(ω), absorption coefficient spectrum $\alpha(\omega)$, reflectivity $R(\omega)$, electron energy-loss spectrum $L(\omega)$, extinction coefficient $k(\omega)$, and optical conductivity σ(ω). A crucial element is the absorption coefficient, which tells us the optimal solar energy conversion efficiency and the amount of light with a given energy or frequency that may pass through a substance before being absorbed. The intensity attenuation of light traveling through a material is described by the absorption coefficient. For an optical process, it can be thought of as the total of the absorption cross-sections per unit volume of a substance. The absorption coefficient rose from 1.64eV to 3.16eV for 0GPa and 20GPa, then slightly decreased before rising sharply from 5.63eV to 8.26eV. As shown in Figure 7(d), the highest peaks for 0GPa and 20GPa are 52.69(ω) and 55.2(ω), respectively. Given that it occurs in the low energy zone and has a broad range of roughly 5eV–16eV, the RbTaO3 appears to have a decent absorption coefficient. As pressure rises, the absorption coefficient increases. The calculated reflectance $R(\omega)$ of the studied compound within the range of 0–18 eV is displayed in Figure 7(e). For 0GPa and 20GPa, respectively. This suggests that within the ultraviolet (UV) spectrum, roughly 33% of the incident light is reflected and 39% can be absorbed. According to the graph, pressure causes the reflectivity $R(0)$ at zero frequency to decrease. Figure 7(c) displays the computed refractive index $n(\omega)$. The static refractive indexes $n(0)$ at zero frequency limit are 3.62 for 0GPa and 4.90 for 40GPa. One crucial optical property that

shows the possibility of quick electron interactions within a material is the electron energy loss function, or $L(\omega)$. In addition to interband transitions, these interactions are responsible for phonon excitation, inner shell ionizations, plasmon excitations, and intraband transitions (Azzouz *et al*., 2019; Hu *et al*. 2007; Murtaza *et al*., 2014). The (ω) for 0GPa has highest distinct peaks at 12.95eV in Figure 7(g). The calculated extinction coefficient $k(\omega)$ for $RbTaO_3$ at 0GPa -20GPa is shown in Figure 7(f). For 20GPa. The peaks are primarily around the ultra-violet regions, and the computed $L(\omega)$ is minimum in the infrared, visible, and lower ultraviolet regions, indicating that $RbTaO_3$ has optical uses. The computation shows that the imaginary part of the dielectric function gets smaller as the amplitude of the energy loss function increases at higher energies. The value of $k(\omega)$ rises with energy in the visible light zone and reaches a maximum of 1.69 at 7.03eV in the UV region. In the high energy zone, the value of $k(\omega)$ begins to decay and become inactive, and as the compound's pressure increases, so do the frequency of $k(\omega)$.

CONCLUSION

we have examined and presented the impact of hydrostatic pressure (0GPa to 150GPa) on the structural, electrical, mechanical, lattice dynamics, and optical characteristics of the cubic perovskite $RbTaO_3$. First, the empirical measurements that relate the stability of the perovskite $RbTaO_3$ to its chemical composition—the tolerance factor (t) and the octahydral factor (μ)—were examined. The compound is regarded as structurally stable since the results for "t" and "μ" meet the requirements. The material is determined to be brittle mechanically based on the B/G ratio and Cauchy relation values. According to the elastic constants requirements, it is also elastically stable against deformation. According to the Zener anisotropy factor data, the compound exhibits anisotropic behavior between 0 and 40 GPa and isotropic behavior above 40 GPa. Furthermore, the bulk modulus data show that the material gets extremely hard when the pressure rises above 40 GPa. It was discovered that the compound's electrical band structures under pressure are entirely semiconductors. As the pressure rose above 150 GPa, a change from an indirect to a direct band gap was noted. The $RbTaO_3$ molecule is a strong candidate for use in optoelectronic, photovoltaic, and photochemistry devices because to its energy band gaps, which fall between 1.4eV and 3.0eV. Using the Thermo_pw algorithm, the compound's lattice dynamics was examined, and imaginary (negative) frequencies in the Brillouin zone were noted. Its dynamic instability is revealed by this trait. Additionally, the different optical quantities are computed and described. It is discovered that the optical band gaps from the absorption coefficient spectrum are near the material's energy band gap.

REFERENCES

Aigbekaen, E.E., and Ighrakpata, F. C. (2022). The First Principal Study Of The Structural, Electronic, Elastic, Vibrational And Thermal Properties Of Cscl Type-Ercu Alloy. *AAN Journal of Sciences, Engineering & Technology Vol. 1, Issue 1, pp. 1-11.*

Azzouz, L., Halit, M., Rera M. T., Khenata A. K., Singh, M., Obeid, M. H., Jappor R., and Wang X. (2019). Structural, electronic and optical properties of $ABTe_2$ (A= Li, Na, K, Rb, Cs and B= Sc, Y, La): Insights from first-principles computations. *Journal of Solid State Chemistry, 279, 120954.*

Bakare, F. O., Babalola, M. I., and Iyorzor, B. E. (2017). The role of alloying elements on the structural, mechanical and thermodynamic properties of Al3X binary alloy system (X = Mg, Sc and Zr): first principle. *Materials Research Express, 4(11), 116502.*

Bouadjemi, B., Bentata, S., Abbad, A., & Benstaali, W. (2015). Ab-initio study of optoelectronic and magnetic properties of the orthorhombic NdMnO3 perovskite. *Solid State Communications, 207, 9-15.*

Boucetta, S. (2014). Theoretical study of elastic, mechanical and thermodynamic properties of MgRh intermetallic compound. *Journal of Magnesium and Alloys, 2 (1) 59-63.* https://doi.org/10.1016/j.jma.2014.04.001

Butt, M. K., Yaseen, M., Ghaffar, A., & Zahid, M. (2020). First principle insight into the structural, optoelectronic, half metallic, and mechanical properties of cubic perovskite $NdInO_3$. *Arabian Journal for Science and Engineering, 45(6), 4967-4974.*

Cheng, B. L., Su, B., Holmes, J. E., Button, T. W., Gabbay, M., & Fantozzi, G. (2002). Dielectric and mechanical losses in (Ba, Sr) TiO_3 systems. *Journal of electroceramics, 9(1), 17-23.*

El Rhazouani, O., Zarhri, Z., Benyoussef, A., & El Kenz, A. (2016). Magnetic properties of the fully spin-polarized Sr $_2CrOsO_6$ double perovskite: A Monte Carlo simulation. *Physics Letters A, 380(13), 1241-1246.*

Giannozzi, P., Andreussi, O., Brumme, T., Bunau, O. , Nardelli, M.B., Calandra, M. , Car, R., cavazzoni, C., Ceresoli, D., Cococcioni, M., and Colonna, N. (2017). Advanced capabilities for materials modelling with

Quantum ESPRESSO. Journal of physics: Condensed matter, 29(46), p.465901.

Hassan, M., Liaqat, M., & Mahmood, Q. (2021). Pressure dependence of electronic, optical and thermoelectric properties of $RbTaO_3$ perovskite. *Applied Physics A, 127(4), 1-8*.

Hu, J. M., Huang, S. P., Xie, Z., Hu, H., & Cheng, W. D. (2007). First-principles study of the elastic and optical properties of the pseudocubic Si_3 As_4, Ge_4 As_4 and Sn_3As_4. *Journal of Physics: Condensed Matter, 19(49), 496215*.

Hussain, M. I., Khalil, R. A., Hussain, F., & Rana, A. M. (2021). DFT-based insight into the magnetic and thermoelectric characteristics of $XTaO_3$ (X= Rb, Fr) ternary perovskite oxides for optoelectronic applications. *International Journal of Energy Research, 45(2), 2753-2765*.

Ilyas, A., Khan, S. A., Liaqat, K., & Usman, T. (2021). Investigation of the structural, electronic, magnetic, and optical properties of $CsXO_3$ (X= Ge, Sn, Pb) perovskites: A first-principles calculations. *Optik, 244, 167536*.

Iyorzor, B. E., Babalola, M. I., Adetunji, B. I. and Bakare, F. O. (2018). Effect of Tellurium333 concentration on the sructural, electronic and mechanical properties of Beryllium Sulphide: DFT approach. *Materials Research Express, 5(5), 056517*.

Iyorzor,B.E., Babalola, M.I., and Aigbekaen,E.E. (2018). Ab initio Calculation of the Structural, Mechanical and Thermodynamic Properties of Beryllium Sulphides, BeS, *J.Appl.Sci.Environ.Manage.,Vol.22(1), 41-46.*

Jindal, S., Vasishth, A., Devi, S., & Anand, G. (2018). A review on tungsten bronze ferroelectric ceramics as electrically tunable devices. *Integrated Ferroelectrics, 186(1), 1-9.*

Khandy, S. A., & Gupta, D. C. (2017). Structural, elastic and magneto-electronic properties of half-metallic BaNpO3 perovskite. *Materials Chemistry and Physics, 198, 380-385*.

Lufaso, M. W., and Woodward, P. M. (2001). Prediction of the crystal structures of perovskites using the software program SPuDS. *Acta Crystallographica Section B: Structural Science, 57(6), 725-738.*

Murtaza, G., Gupta, S. K., Seddik, T., Khenata, R., Alahmed, Z. A., Ahmed, R., Khachai H, Jha P. K. and Omran, S. B. (2014). Structural, electronic, optical and thermodynamic properties of cubic REGa3 (RE= Sc or Lu) compounds: Ab initio study. *Journal of alloys and compounds, 597, 36-44*.

Okunzuwa, I. S., and Aigbekaen, E.E. (2021). Structural Optimization, Electronic Band Structure, Mechanical and Thermodynamics Properties of Fe3 Al. *Physical Science International (JournalArticle no.PSIJ.67620) 25(2): 1-11*.

Okunzuwa, S., and Aigbekaen, E. (2020). Structural Optimization and the Study of the Electronic, Mechanical, Thermodynamic and Phonon Properties of Mg2Sn from First Principle. *Physical Science International (JournalArticle no.PSIJ.67620) 24(12): 60-71*.

Perdew, J.P., Burke, K., and Ernzerhof, M. (1996). Generalized gradient approximation made simple. *Phys. Rev. Lett. 77, 3865–3868.*

Perdew, J.P., Burke, K., and Ernzerhof, M. (1997). Generalized gradient approximation made simple. *Phys. Rev. Lett. 78, 1396*.

Pithan, C., Hennings, D., & Waser, R. (2005). Progress in the synthesis of nanocrystalline $BaTiO_3$ powders for MLCC. *International Journal of Applied Ceramic Technology, 2(1), 1-14*.

Pugh, S.F. (1954). Relations between the Elastic Moduli and the Plastic Properties of Polycrystalline Pure Metals. *The London, Edinburgh and Dublin Philosophical Magazine and Journal of Science, 45, 823-843*

Raveau, B., Maignan, A., Martin, C., & Hervieu, M. (1998). Colossal magnetoresistance manganite perovskites: relations between crystal chemistry and properties. *Chemistry of materials, 10(10), 2641-2652.*

Reshak, A. H. (2016). Transport properties of the n-type $SrTiO_3$/$LaAlO_3$ interface. *RSC Advances, 6(95), 92887-92895.*

Sarwan, M., Shukla, P., & Singh, S. (2020). Structural stability, electronic and elastic properties of cubic $RbTaO_3$ perovskite oxide. *In AIP Conference Proceedings (Vol. 2265, No. 1, p. 030341). AIP Publishing LLC.*

Schneemeyer, L. F., Waszczak, J. V., Zahorak, S. M., van Dover, R. B., & Siegrist, T. (1987). Superconductivity in rare earth cuprate perovskites. *Materials research bulletin, 22(11), 1467-1473*.

Sinko, G.V., and Smirnow, N.A. (2002). Ab initio Calculations of Elastic Constants and Thermodynamic Properties of bcc, fcc, and hcp Al Crystals under Pressure. *Journal of Physics: Condensed Matter, 14, 6989-7005.* https://doi.org/10.1088/0953-8984/14/29/301

Tahiri, O., Kassou, S., & Mrabet, R. (2018). First principles calculations of electronic and optical properties for mixed perovskites: Ba (1-x) Ca (x) TiO_3 and Ba (1-x) Sr (x) TiO_3 (x= 0.4, 0.6). *Materials and Devices, 3, 2004-2018*.

Tian, Z., Wang, X., Shu, L., Wang, T., Song, T. H., Gui, Z., & Li, L. (2009). Preparation of nano $BaTiO_3$-based ceramics for multilayer ceramic capacitor application by chemical coating method. *Journal of the American Ceramic Society, 92(4), 830-833*.

Tsurumi, T., Adachi, H., Kakemoto, H., Wada, S., Mizuno, Y., Chazono, H., & Kishi, H. (2002). Dielectric properties of $BaTiO_3$-based ceramics under high electric field. *Japanese journal ofapplied physics, 41(11S), 6929.*

Wu, Z., Hao, X., Liu, X., and Meng, J. (2007). Structures and elastic properties of investigated via first-principles density functional calculations. *Phys. Rev. B. 75(5), 054115*.